Clinical and Experimental Obstetrics & Gynecology

Clin. Exp. Obstet. Gynecol. **2026**; 53(3): 45232
https://doi.org/10.31083/CEOG45232

Original Research

Performance of a Deep Learning-Based Fetal Magnetic Resonance Imaging System in the Assessment of Fetal Growth Restriction and Placental Insufficiency

Yujin Zhang[1,*], Kaiming Li[1], Xiangao Lei[1], Bo Zhang[2], Fumin Zhao[1]

[1]Department of Radiology, West China Second University Hospital, Sichuan University, 610041 Chengdu, Sichuan, China
[2]Department of Ultrasound, West China Second University Hospital, Sichuan University, 610041 Chengdu, Sichuan, China
*Correspondence: Bridgejin123@163.com (Yujin Zhang)

Academic Editor: Paolo Ivo Cavoretto
Submitted: 23 July 2025 Revised: 30 October 2025 Accepted: 14 November 2025 Published: 23 March 2026

Abstract

Background: Fetal growth restriction (FGR) and placental insufficiency (PI) are major contributors to adverse perinatal outcomes, and early identification remains clinically challenging. This study aimed to evaluate the utility of artificial intelligence (AI)-based fetal magnetic resonance imaging (MRI) for early screening of FGR and PI. **Methods**: A retrospective analysis was conducted on 120 pregnant women with a gestational age of 24–36 weeks who underwent fetal MRI examinations at the Second Hospital of West China, Sichuan University, from September 2024 to May 2025. Participants were divided into an FGR group, defined by an estimated fetal weight (EFW) below the 10th percentile for gestational age based on the Hadlock growth chart (n = 60), and a non-FGR group, defined by an EFW at or above the 10th percentile for gestational age (n = 60). MRI examinations were performed using a 3.0-T MRI Premier scanner with a 32-channel Head GE AIR™ Coil body coil, acquiring T2-weighted single-shot fast spin-echo (SSFSE) sequences of the fetal abdomen and placenta. Accelerated protocol images were reconstructed using the AIR™ Recon Deep Learning (DL) algorithm. FGR assessment relied on EFW, calculated from U-Net-segmented fetal abdominal volume combined with ultrasound-measured fetal femur length (FL) using the Hadlock formula, and compared with birth weight. EFW below the 10th percentile for gestational age served as the criterion for FGR. Segmentation performance was evaluated using the Dice similarity coefficient (target >0.85), diagnostic accuracy via the area under the receiver operating characteristic (ROC) curve (AUROC), and EFW error via mean absolute error (MAE, target <150 g). Ultrasound FL measurements were performed using a GE Voluson E10 system by certified sonographers, following the International Society of Ultrasound in Obstetrics and Gynecology (ISUOG) guidelines, within 3 days of MRI to ensure consistency. **Results**: AIR™ Recon DL-reconstructed images achieved a signal-to-noise ratio (SNR) of 59.5 $\pm$ 7.1 and a contrast-to-noise ratio (CNR) of 26.9 $\pm$ 4.8, significantly higher than non-reconstructed images ($p < 0.05$). The Dice coefficient for placental and fetal structure segmentation was 0.892 $\pm$ 0.021, the EFW MAE was 148.2 g, and FGR diagnostic accuracy was 91.7% (AUROC = 0.938), outperforming manual assessment (84.5%, AUROC = 0.864; $p = 0.032$). In the FGR with PI subgroup, diagnostic accuracy reached 93.4%, with an MAE of 135.6 g ($p = 0.016$). **Conclusions**: Fetal MRI combined with the AIR™ Recon DL algorithm shows significant clinical value in assessing FGR and PI. This system enhances image quality, accelerates scanning, and reduces artifacts, thus improving the accuracy of FGR and PI diagnosis in early screening. This technique also offers reliable support for early screening and the development of individualized treatment plans in the context of high-risk pregnancy.

Keywords: deep learning; fetal growth retardation; placental insufficiency; magnetic resonance imaging; image enhancement; artificial intelligence

1. Introduction

Fetal growth restriction (FGR) and placental insufficiency (PI), two common complications during gestation, are closely linked to fetal health and prognostic outcomes [1,2]. FGR refers to a fetal weight below the 10th percentile for gestational age, whereas FGR denotes growth restriction triggered by PI or other pathological factors [3]. The occurrence of FGR is often correlated with preterm delivery, low birth weight (LBW), neonatal asphyxia, neurodevelopmental disorders, and other adverse outcomes, standing as a high-risk factor during pregnancy [4]. PI, a leading pathogenic factor for FGR, severely disrupts normal fetal growth and development by impairing oxygen delivery and nutrient exchange.

Accurate early diagnosis of FGR and PI is crucial for reducing fetal complications and enhancing pregnancy outcomes. Early identification and intervention allow clinicians to develop individualized treatment regimens, hence effectively preventing or mitigating adverse pregnancy outcomes. However, conventional assessment methods, like ultrasound, computed tomography (CT), and routine magnetic resonance imaging (MRI), have certain limitations in specific contexts [5,6]. Ultrasound is widely used for FGR and PI screening; however, it has limited accuracy for assessing placental function and early symptoms of FGR in certain situations due to operator dependence, equipment performance, fetal position, amniotic fluid volume (AFV), and other technical factors [7]. CT is accompanied by ioniz-

ing radiation risks, making it generally unsuitable for pregnant women and fetuses [8]. Moreover, while conventional MRI provides excellent soft tissue contrast, it remains susceptible to fetal motion artifacts and requires prolonged acquisition times, limiting its utility for detailed visualization of the placenta and fetal structures [9].

Traditional imaging methods have long served as the primary approaches for the assessment of FGR and PI, among which ultrasound is the most prevalent. Ultrasound evaluates fetal health by estimating fetal weight and measuring placental blood flow. Nevertheless, image quality of ultrasound images usually fluctuates with operator experience and equipment performance, which limits the accuracy of FGR detection and placental function assessment. For example, fetal weight estimation using ultrasound depends on fetal volume and image clarity, both of which may be influenced by changes in AFV, fetal position, and other factors, hence affecting the accuracy of measurements [10].

As a radiation-free imaging modality, MRI demonstrates distinct advantages for the FGR and PI assessment due to its high-resolution soft tissue images. This technique provides clear visualization of placental and fetal anatomical structures, playing an irreplaceable role in the imaging of vital organs like the brain and heart for fetuses, particularly in complex cases. However, this traditional method also has clear limitations. Conventional MRI, however, remains affected by equipment performance, fetal motion, and prolonged acquisition times, which collectively limit image quality and diagnostic reliability. Therefore, strategies that address these limitations and enhance the clinical value of MRI in evaluating FGR and PI represent important research goals [11].

Over recent years, deep learning (DL) techniques, especially convolutional neural network (CNN), have achieved substantial progress in medical imaging field applications [12,13]. DL can emulate neural processing in the human brain and efficiently extract image features for further classification, testing, and reconstruction, which supports image quality enhancement, automated diagnosis, and disease prediction [14,15]. In the field of MRI, DL is mainly adopted for image reconstruction and denoising to improve image quality, shorten scan time, and lessen artifacts [16]. Specifically, this technology enables effective denoising of images with low signal-to-noise ratio (SNR) and enhances image resolution by learning features from large-scale imaging datasets, which improves diagnostic accuracy [17,18]. In addition to enhancing image details, DL can also improve image contrast, performing particular effectiveness in fetal and placental image reconstruction. Furthermore, DL can automatically identify lesions or abnormalities, assisting clinicians in more accurately assessing fetal and placental health.

Previous studies have also explored DL-based fetal segmentation and estimated fetal weight (EFW) prediction. Specktor-Fadida *et al*. [14] developed a DL-based whole-body fetal MRI segmentation framework for MRI-based fetal weight estimation, achieving high segmentation performance (Dice = 0.973) and high accuracy with a mean difference between MRI-estimated fetal weight (EFW) and birth weight of –0.39%. Knoll *et al*. [19] optimized a 3D U-Net model for fetal brain segmentation with high reproducibility, while Sobhaninia *et al*. [20] proposed a multi-task DL approach for fetal ultrasound biometry. However, most of these studies have focused on single-modality segmentation (MRI or ultrasound), without integrating DL-based image reconstruction or placental function analysis. Therefore, clinically validated frameworks combining DL-enhanced MRI reconstruction with fetal body segmentation and EFW prediction remain limited.

Since the introduction of the AIR™ Recon DL algorithm by General Electric (GE), DL-based reconstruction methods have greatly improved MRI image quality [21]. By optimizing the image reconstruction process, AIR™ Recon DL can effectively denoise images and enhance fine details [22], demonstrating substantial advantages especially in fetal and placental imaging. Studies have shown that AIR™ Recon DL can accelerate scanning, reduce the scanning duration of conventional MRI, and boost the quality of images with low SNR, thereby providing clearer visualization of fetal and placental structure details [16,22]. Thus, fetal MRI using this algorithm on 3.0-T SIGNA™ Premier equipment can provide higher quality images and more precise information for the early diagnosis of FGR and PI.

The primary aim of this study is to evaluate the diagnostic performance and image quality improvement achieved by the built-in AIR™ Recon DL reconstruction algorithm in fetal MRI using the GE 3.0-T SIGNA™ Premier system. Specifically, this study focuses on validating the algorithm's impact on image quality, artifact reduction, and diagnostic efficiency for FGR and PI.

2. Materials and Methods

2.1 Study Design and Sample Selection

This study was designed to evaluate the utility of artificial intelligence (AI)-based fetal MRI for the early screening of FGR and PI (Fig. 1). Specifically, the study aimed to validate the diagnostic performance of the built-in AIR™ Recon DL reconstruction algorithm, rather than to develop a new CNN model. The study population consisted of pregnant women undergoing fetal MRI examinations at the Obstetrics Department of West China Second University Hospital from September 2024 to May 2025. All participants carried singleton pregnancies. Based on the diagnostic criterion for FGR (EFW below the 10th percentile for gestational age), participants were assigned to an FGR group. This diagnostic threshold follows the clinical guidelines issued by the International Society of Ultrasound in Obstetrics and Gynecology (ISUOG), which define FGR as an EFW below the 10th percentile for gestational age [10]. Although all eligible participants were consecutively enrolled, to minimize the potential influence of gestational age on group comparisons and to maintain statistical balance,

frequency matching by gestational age was applied during analysis. This approach resulted in equal numbers of participants in the FGR and non-FGR groups (n = 60 each), totaling 120 participants. The sample size was determined via power calculation (α = 0.05, power = 0.8) to detect a 15% difference in FGR diagnostic accuracy.

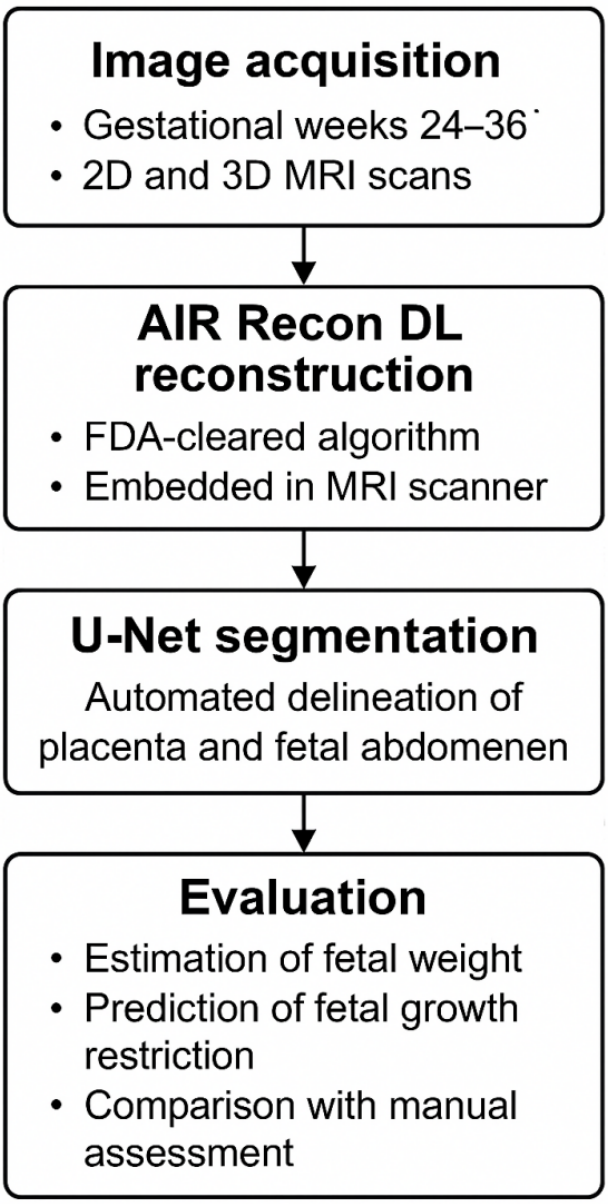

Fig. 1. Flowchart of the study pipeline for AI-based fetal MRI using the AIR™ Recon DL algorithm. AI, artificial intelligence; MRI, magnetic resonance imaging; DL, deep learning.

This retrospective study was reviewed and approved by the Institutional Review Board (IRB) of the Medical Research Ethics Committee of the Second Hospital of West China, Sichuan University (Approval No. 313, 2024). The requirement for written informed consent was formally waived by the IRB due to the retrospective nature of the study. All procedures were conducted in accordance with the Declaration of Helsinki and applicable national regulations.

Inclusion criteria were: (1) gestational age of 24–36 weeks; (2) absence of severe complications (e.g., malignant tumors, or endocrine disorders); and (3) MRI examinations of acceptable diagnostic quality without severe motion artifacts. Only fetuses without major structural or chromosomal abnormalities were included to ensure dataset homogeneity. Exclusion criteria included: (1) severe fetal anomalies; (2) MRI contraindications (e.g., implanted metal devices); and (3) inability to tolerate scanning.

FGR diagnosis was defined as an EFW below the 10th percentile for gestational age based on the Hadlock growth chart, which was also used to establish percentile thresholds for postnatal birthweight confirmation [10]. Cases were retrospectively reviewed, and final FGR classification was supported by birthweight percentiles and available prenatal Doppler findings, including an umbilical artery pulsatility index >95th percentile or a cerebroplacental ratio (CPR) <5th percentile. Neonatal outcomes, such as LBW (<2500 g) and Neonatal Intensive Care Unit (NICU) admission, were also recorded for reference [3,5,10]. PI was defined according to abnormal Doppler parameters, including an umbilical artery pulsatility index >95th percentile and/or a CPR <5th percentile for gestational age, consistent with ISUOG recommendations [10]. In cases where Doppler data were unavailable, PI diagnosis was supported by MRI findings, such as reduced placental volume or elevated placental T2 values, and by adverse perinatal outcomes, such as LBW or NICU admission [5].

During the study period, 156 pregnant women underwent fetal MRI examinations. Of these, 132 met the inclusion criteria, and 120 were ultimately analyzed after excluding cases with incomplete data or poor image quality.

2.2 Data Collection and Image Acquisition

All fetal MRI examinations were conducted using a 3.0-T MRI scanner (SIGNA™ Premier, GE Healthcare, Chicago, IL, USA) equipped with a 32-channel GE AIR™ Coil body coil for signal reception. The coil's high sensitivity and uniform signal coverage optimized the SNR and contrast-to-noise ratio (CNR), while effectively minimizing fetal motion artifacts during imaging of the placenta and fetal abdomen. The standard fetal MRI protocol included axial T2-weighted fat-saturated (FS) single-shot fast spin-echo (SSFSE), axial T1-weighted gradient-echo, sagittal T2-weighted SSFSE, coronal T2-weighted SSFSE, and three-dimensional (3D) T2-weighted sequences to capture images of the placenta and fetal abdomen. Both two-dimensional (2D) and 3D acquisitions were performed to assess volumetric reconstruction and segmentation. FGR assessment relied on MRI-derived fetal abdominal volume combined with fetal femur length (FL) measured via ultrasound to calculate EFW. Ultrasound examinations were performed using a GE Voluson E10 ultrasound system (GE HealthCare, Zipf, Austria) by certified sonographers with

at least 5 years of fetal ultrasound experience, following standardized biparietal diameter and FL measurement protocols, as per ISUOG guidelines [10]. MRI and ultrasound examinations were conducted within the same gestational week (24–36 weeks), with a maximum interval of 3 days to ensure data consistency. Doppler ultrasound was performed within three days of MRI acquisition to measure the umbilical artery pulsatility index, middle cerebral artery PI, and to calculate the CPR. All examinations were performed by certified obstetric sonographers following ISUOG standards for fetal Doppler assessment [10].

The standard MRI protocol had an average scanning time of 18 minutes and 45 seconds, while an accelerated protocol averaged 7 minutes and 30 seconds. Raw accelerated MRI images were transferred to post-processing software (Orchestra SDK, GE Healthcare) and reconstructed using the AIR™ Recon DL algorithm, with reconstructed images labeled as DL sequences. The AIR™ Recon DL pipeline incorporates a deep CNN with approximately 10,000 kernels and 4.4 million trainable parameters. Importantly, this CNN is an FDA (Food and Drug Administration)-cleared, commercially embedded algorithm within the GE scanner, rather than a newly developed research model. The CNN processes raw complex-valued imaging data to generate high-quality output images by: (1) reducing user-adjustable image noise, (2) minimizing truncation artifacts, and (3) enhancing edge sharpness. Integration into the scanner's native inline reconstruction pipeline ensures access to raw, full-bit-depth data. The CNN was trained using supervised learning with image pairs consisting of near-perfect high-resolution images (minimal ringing, low noise) and conventional images synthesized to include higher noise and truncation artifacts. In our study, the use of AIR™ Recon DL under the same acquisition protocol reduced the mean scan time by approximately 60% while maintaining equivalent spatial resolution. The cohort-specific SNR increased by 92% $\pm$ 11% compared with non-DL sequences, consistent with vendor specifications. Motion artifact reduction was quantified using a 5-point artifact severity scale (1 = severe, 5 = minimal), showing an improvement from 3.1 $\pm$ 0.6 to 4.2 $\pm$ 0.5 ($p < 0.01$).

This denoising and edge-enhancement capability further improved the diagnostic quality of MRI images that were acceptable but not entirely free of motion artifacts. To assess consistency and reproducibility, two independent radiologists evaluated 30 randomly selected MRI studies twice, separated by a 2-week interval, and inter-observer and intra-observer agreement were calculated using intra-class correlation coefficients (ICCs). Ultrasound data were stored in Digital Imaging and Communications in Medicine (DICOM) format and, together with MRI images, transferred to the Picture Archiving and Communication System (PACS; IMPAX 6, Agfa-Gevaert NV) for further analysis.

2.3 Data Preprocessing and Segmentation

MRI image datasets were exported from the PACS and preprocessed using ITK-SNAP (version 3.8) for registration, denoising, and standardization. Segmentation of the placenta and fetal abdomen was performed using a 2D U-Net model, trained on an NVIDIA RTX 3090 GPU for 100 epochs with a cross-entropy loss function and a learning rate of 0.001. The Adam optimizer ($\beta_1 = 0.9$, $\beta_2 = 0.999$) was used, with a batch size of 8 and early stopping applied after 20 epochs without validation improvement. Data augmentation included random rotation ($\pm$10°), horizontal and vertical flipping, and intensity scaling ($\pm$10%) to improve model generalization.

The training dataset comprised images from 80 pregnant women (67%), with validation and test sets each including images from 20 pregnant women (16.7%). To ensure subject-level independence, all images from a single subject were assigned to only one subset. Segmentation masks were annotated by two radiologists (Kappa = 0.85). In addition, inter-rater reliability was further assessed using Dice overlap (mean = 0.87 $\pm$ 0.03) and Bland–Altman analysis, confirming strong agreement between observers. The 2D U-Net model utilized AIR™ Recon DL-reconstructed T2-weighted SSFSE images as input to generate masks for the placenta and fetal abdomen. This segmentation model was implemented exclusively for automated region delineation and not for diagnostic classification of abnormalities. When the Dice similarity coefficient (DSC) was $<$0.80, manual correction was performed by two radiologists according to predefined anatomical rules: (1) placental boundaries were delineated along the T2-weighted hypointense edge, excluding maternal myometrium; (2) fetal abdominal contours were refined to exclude umbilical cord and amniotic fluid. Disagreements were resolved through consensus review.

Fetal FL was measured via ultrasound using standardized ISUOG measurement protocols [10], and the data were input as numerical values into the subsequent EFW calculation model. FGR identification was based on EFW calculated from MRI-segmented fetal abdominal volume and ultrasound-measured FL, using the Hadlock formula, compared against birth weight, with EFW below the 10th percentile serving as the criterion for FGR prediction. Segmentation performance was evaluated using the Dice similarity coefficient (target $>$0.85), with manual correction applied as described above. EFW prediction error was assessed using MAE (target $<$150 g, along with accuracy, sensitivity, specificity, and area under the receiver operating characteristic (ROC) curve (AUROC).

2.4 Model Training and Assessment

For the segmentation model, datasets were divided into training, validation, and test subsets (80, 20, and 20 subjects, respectively), as described in Section 2.3. For the subsequent regression model used for EFW prediction and FGR identification, data from 120 subjects were divided at

the subject level into training (80%) and validation (20%) subsets, and five-fold cross-validation was applied to enhance model generalization.

Placental and fetal abdominal segmentation was performed using the 2D U-Net model, while the EFW prediction model integrated MRI-segmented abdominal volume and ultrasound-measured FL data using a regression framework based on the Hadlock formula. No additional CNN or classification networks were trained or fine-tuned in this study; all reconstructions were performed using the manufacturer-implemented AIR™ Recon DL algorithm. The regression model was trained to minimize prediction error between MRI-based EFW and actual birth weight. To prevent potential temporal bias, datasets were randomly partitioned according to acquisition date to ensure chronological independence between training and validation samples. Fold-wise performance metrics were averaged across five folds, and 95% confidence intervals (CIs) were calculated to assess model stability.

Evaluation metrics included the Dice similarity coefficient (target >0.85) for placental segmentation, MAE (target <150 g for EFW prediction, root mean square error (RMSE), coefficient of determination (R^2), and AUROC for FGR identification. All reported performance values were obtained from the validation and independent test sets corresponding to each model. As this was a single-center study using one MRI scanner, potential institutional bias and limited generalizability should be acknowledged, and further external validation is warranted.

2.5 Comparison With Manual Assessment

2.5.1 DL System's FGR Identification Performance

The FGR identification function of the DL system was based on a comparison between the EFW, calculated by integrating MRI-segmented fetal abdominal volume and ultrasound-measured FL, with the actual birth weight. Using an EFW below the 10th percentile as the criterion for FGR prediction, the accuracy, sensitivity, specificity, and AUROC of the DL system were calculated.

2.5.2 Performance of Manual Assessment in FGR Identification

The manual assessment was carried out by 2 senior radiologists separately. The physicians completed fetal weight assessment and placental function analysis as per routine imaging criteria, with the same diagnostic criteria for FGR. Comparisons were made between the assessment results and the diagnostic results from the DL system, and the accuracy, sensitivity, specificity, and AUROC of the manual and system results were calculated.

The reference placental volume used for error analysis was obtained from manual segmentation performed by two experienced radiologists using ITK-SNAP software (version 3.8, www.itksnap.org). Each segmentation was performed independently and subsequently reviewed jointly to reach consensus. The mean of the two measurements was considered the actual placental volume for comparison with the system-estimated volume.

2.6 Statistical Analysis

All statistical analyses were performed using SPSS software (version 26.0, IBM, Armonk, NY, USA). Image quality metrics (SNR, CNR, and edge sharpness scores) were compared between AIR™ Recon DL-reconstructed and non-reconstructed images using paired *t*-tests. For intergroup comparisons of continuous variables (e.g., per-case Dice Dcoefficients), independent-samples *t*-tests or Mann–Whitney U tests were applied according to the Shapiro–Wilk normality test. The "Consistency of placental volume measurement" reported in Table 3 represents a reliability coefficient (ICC). Because this metric is a statistical coefficient rather than a continuous variable, it was summarized descriptively (0.85 vs. 0.93). The *p*-value reflects a comparison of these coefficients using Fisher's z-transformation rather than a *t*-test.

For Table 4, per-case continuous outcomes, such as placental-volume estimation error, were analyzed using paired *t*-tests or nonparametric alternatives. Summary performance metrics, such as accuracy and AUROC, were not treated as continuous variables; AUROC values were compared using DeLong's test.

Placental segmentation performance was assessed via the Dice similarity coefficient, and the diagnostic accuracy for FGR and PI was evaluated using ROC curve analysis with AUROC calculation (AUROC). For each key metric (AUROC, MAE, and Dice coefficient), 95% CIs were computed to assess statistical precision and robustness. Comparisons between the AUROC values of the DL system and manual assessment were performed using DeLong's test. Multiple comparisons across subgroups were adjusted using the Benjamini–Hochberg false discovery rate (FDR) correction method to control type I error inflation. Correlations between MRI-derived placental parameters (e.g., placental volume, mean T2 value) and Doppler indices (umbilical artery PI, CPR) were assessed using Pearson or Spearman correlation coefficients, depending on data distribution.

EFW prediction error was evaluated using MAE, with a target MAE below 150 g. All statistical tests were two-sided, with significance thresholds adjusted for multiple comparisons (adjusted $p < 0.05$). Results are presented as mean ± standard deviation (SD) or mean (95% CI), as appropriate.

3. Results

3.1 Baseline Characteristics of Patients

A total of 120 pregnant women who underwent fetal MRI were included in the study and were grouped according to the presence of FGR: the FGR group (n = 60) and the non-FGR group (n = 60). The two groups showed no significant differences in baseline characteristics, including gestational age and maternal age ($p > 0.05$). In the FGR group,

Table 1. Comparison of patient baseline characteristics (mean ± SD).

Indicators	FGR group (n = 60)	Non-FGR group (n = 60)	95% CI (FGR / Non-FGR)	*p*-value
Gestational age (weeks)	31.2 ± 2.3	31.6 ± 2.0	(30.6–31.8) / (31.1–32.1)	0.296
Maternal age (years)	29.8 ± 3.7	30.2 ± 3.4	(28.9–30.7) / (29.3–31.1)	0.512
EFW (g)	1230.6 ± 215.4	1685.9 ± 245.3	(1176–1285) / (1624–1748)	<0.001
Placental volume (cm^3)	310.7 ± 44.2	391.5 ± 47.8	(299–322) / (379–404)	<0.001
Placental T2 value (ms)	87.4 ± 8.9	101.2 ± 9.5	(85.1–89.7) / (98.8–103.6)	<0.001
Birth weight (g)	2145.8 ± 345.7	2923.3 ± 312.1	(2058–2233) / (2844–3002)	<0.001

Note: FGR, fetal growth restriction; CI, confidence interval; EFW, estimated fetal weight; T2, transverse relaxation time; SD, standard deviation.

Table 2. System segmentation and predictive indicators.

Items	Values	95% CI
Dice coefficient of placental segmentation	0.892 ± 0.021	0.888–0.896
Intersection over union (IoU) of placental segmentation	0.821 ± 0.034	0.814–0.828
EFW MAE (g)	148.2	139.6–156.8
EFW RMSE (g)	192.6	180.2–205.0
Predicted R^2	0.86	0.82–0.90
FGR identification accuracy	91.70%	88.5–94.9
AUROC	0.938	0.912–0.964
Sensitivity/specificity	88%/93%	(82–94) / (89–97)

Note: Dice, Dice similarity coefficient; IoU, intersection over union; CI, confidence interval; EFW, estimated fetal weight; MAE, mean absolute error; RMSE, root mean square error; R^2, coefficient of determination; AUROC, area under the receiver operating characteristic curve.

placental volume, EFW, and T2 values were significantly lower than those in the control group, along with significant differences observed in the birth weight (Table 1).

3.2 Assessment of Model Segmentation Performance and Prediction Capability

High-precision segmentation of the placenta and fetal brain structures was achieved using the fetal MRI image analysis system based on DL. The Dice coefficient for placental segmentation was 0.892 ± 0.021, and the MAE for fetal weight estimation reached 148.2 g, indicating good predictive performance, with an R^2 value of 0.86 (Table 2).

3.3 Contribution of AIR™ Recon DL Image Reconstruction to the MRI System

All MRI images were collected through the GE SIGNA™ Premier 3.0-T system, with the AIR™ Recon DL image reconstruction algorithm applied. This algorithm enhances image SNR and CNR based on raw k-space data and attenuates Gibbs artifacts. Comparison of 20 cases before and after applying AIR™ Recon DL found noticeable enhancement in image quality and subsequent segmentation performance (Table 3).

3.4 System and Manual Assessment Comparison

The MRI system based on deep learning demonstrated significant advantages were observed in the FGR identification task. The system achieved an accuracy of 91.7%, substantially higher than the 84.5% of manual assessment. Additionally, the system showed a superior performance in predicting placental volume and identifying placental perfusion abnormalities compared with manual assessment. Combining the two methods further increased the accuracy to 92.2%. See Table 4.

3.5 Performance in Different Risk Subgroups

We analyzed subgroups with different FGR and PI conditions. The system demonstrated superior performance in the FGR + PI group, showing the lowest EFW error (135.6 g) and an FGR detection accuracy of 93.4%. These results suggest that this system has greater application value in high-risk pregnant populations (Table 5).

4. Discussion

This study aimed to evaluate the clinical value of the AIR™ Recon DL algorithm in the assessment of FGR and PI. Our results showed that the AIR™ Recon DL algorithm significantly improved fetal MRI image quality, as evidenced by heightened SNR and CNR. This finding is consistent with preceding study findings, suggesting that DL can effectively reduce motion artifacts and noise generated in traditional imaging methods and enhance image spatial resolution [23–25]. Previous studies have shown that deep learning-based reconstruction can effectively reduce image noise and improve image clarity, thereby mitigating motion-related artifacts and improving diagnostic image quality [21,22]. Consistent with their results, our study further validates these advantages in the context of FGR and PI. Moreover, by integrating MRI-based volumet-

Table 3. Comparison of image quality before and after AIR™ Recon DL reconstruction.

Indicators	Without DL reconstruction (n = 20)	With AIR™ Recon DL (n = 20)	*p*-value	95% CI (DL vs non-DL)
SNR	46.2 ± 8.3	59.5 ± 7.1	<0.001	(43.5–48.9) / (57.1–61.9)
CNR	19.7 ± 5.5	26.9 ± 4.8	<0.001	(18.2–21.2) / (25.6–28.2)
Placental border clarity score (1–5 points)	3.2 ± 0.6	3.9 ± 0.4	0.003	–
Consistency of placental volume measurement	0.85	0.93	0.018	–
Improvement in segmentation Dice coefficient	0.871 ± 0.028	0.908 ± 0.024	<0.01	0.018

Note: AIR™ Recon DL, Adaptive Image Reconstruction Deep Learning; DL, deep learning; SNR, signal-to-noise ratio; CNR, contrast-to-noise ratio; Dice, Dice similarity coefficient. Edge sharpness and placental border clarity were scored by two blinded radiologists using a validated 5-point scale (1 = poor, 5 = excellent). Placental border clarity score (1–5) was analyzed as a continuous variable due to its quasi-continuous distribution, consistent with common imaging-quality assessment practices. The comparison was performed on a paired subset of 20 cases randomly selected from the overall study cohort (the same subjects scanned before and after AIR™ Recon DL reconstruction).

Table 4. System and manual assessment comparison.

Items	Manual (n = 120)	MRI system (n = 120)	Manual + system (n = 120)	*p*-value (system vs. manual)	95% CI (Manual/System)
FGR identification accuracy (%)	84.50%	91.70%	92.20%	0.032	(80.2–88.8) / (88.5–94.9)
AUROC	0.864	0.938	0.944	0.041	(0.822–0.906) / (0.912–0.964)
Placental volume estimation error (cm^3)	42.7 ± 15.2	39.3 ± 14.5	38.6 ± 13.9	0.118	(38.3–47.1) / (35.0–43.6)

Note: MRI, magnetic resonance imaging.

ric analysis with ultrasound-derived biometric parameters, our work expands the application of AIR™ Recon DL from image optimization to comprehensive multimodal evaluation of fetal growth and placental function. With regards to placental and fetal structure visualization, the image clarity achieved by this algorithm was superior to that of traditional MRI reconstruction. The AIR™ Recon DL algorithm further enhanced image usability by applying DL to raw k-space data, enabling more accurate assessment of fetal growth and placental function.

Previous studies have investigated DL-based fetal segmentation and EFW prediction using MRI and ultrasound modalities. Specktor-Fadida *et al*. [14] developed a whole-body fetal MRI segmentation framework that achieved a Dice coefficient of approximately 0.87 and an EFW MAE within 160 g. Knoll *et al*. [19] optimized a 3D U-Net model for fetal brain segmentation, while Sobhaninia *et al*. [20] implemented a multi-task DL approach for fetal ultrasound biometry. However, these studies mainly focused on single-modality imaging and did not integrate DL-based MRI reconstruction or placental function analysis. In contrast, our study integrates DL-enhanced MRI with ultrasound-based biometric data and provides a validated clinical evaluation of FGR and PI. This multimodal framework therefore extends previous segmentation and EFW estimation approaches toward a and clinically applicable diagnostic workflow.

Here, the AIR™ Recon DL algorithm enabled efficient segmentation of the placenta, achieving a Dice coefficient of 0.892, markedly higher than that of traditional image reconstruction methods [18,19]. Placental volume serves as a significant indicator of fetal health, showing substantial clinical significance particularly in examining PI [26]. By using the DL algorithm, placental volume can be measured more accurately, providing strong support for the early diagnosis of FGR and PI.

By integrating high-resolution fetal abdominal MRI with ultrasound-measured fetal FL, this study overcame the limitation of not acquiring fetal femur MRI data, significantly enhancing the clinical utility of EFW predictions. MRI, leveraging its superior soft tissue resolution and the image optimization capabilities of the AIR™ Recon DL algorithm (SNR 59.5 ± 7.1, CNR 26.9 ± 4.8), enabled precise segmentation of the fetal abdomen (Dice coefficient 0.892 ± 0.021), providing reliable abdominal volume data. Ultrasound, as a noninvasive and real-time imaging modality, offers operational simplicity and standardization (following ISUOG guidelines [10]) for measuring fetal FL, a key parameter widely used in FGR assessment [12]. By integrating MRI-derived abdominal volume and ultrasound-measured FL using the Hadlock formula [27], this study achieved high-precision EFW prediction (MAE 148.2 g), offering robust support for the early diagnosis of FGR and PI. However, integrating MRI and ultrasound data requires ensuring temporal consistency (this study limited the inter-

Table 5. Predictive performance in different placental function subgroups.

Subgroups	Predicted MAE (g)	R^2	FGR detection accuracy	95% CI (MAE / Accuracy)	*p*-value (vs. non-PI group)
Non FGR + normal function	152.4	0.84	89.20%	(140–165) / (85.0–93.4)	–
Non FGR + PI	158.3	0.81	85.10%	(145–172) / (80.2–90.0)	0.229
FGR + normal function	141.2	0.86	90.00%	(130–152) / (86.0–94.0)	0.118
FGR + PI	135.6	0.88	93.40%	(125–146) / (89.8–97.0)	0.016

Note: PI, placental insufficiency; MAE, mean absolute error.

val to within 3 days) to minimize variability due to fetal growth. Additionally, operator-dependent variability in ultrasound measurements may introduce errors, which can be mitigated through standardized protocols and experienced sonographers [10,12].

Moreover, the system demonstrated strong performance in predicting fetal weight. The MAE reached 148.2 in our study. Compared with conventional ultrasound-based fetal weight estimation, our approach showed improved predictive performance [27]. This observation confirms that DL-based MRI image reconstruction performs well in anatomical structure assessment and fetal growth assessment with high accuracy. This high-precision weight prediction method is crucial for early-stage FGR and PI detection and can offer strong and reliable evidence for clinical interventions.

This study unraveled that the AIR™ Recon DL algorithm excelled in identifying FGR, achieving an accuracy of 91.7% and an AUROC of 0.938. Compared with the manual method, the system combined with the DL model showed a better performance, with diagnostic accuracy particularly enhanced in high-risk pregnant populations. Currently, FGR diagnosis primarily depends on clinical experience and traditional imaging methods, but they are confronted with various challenges during early-stage diagnosis, such as quality restriction and fetal motion artifacts [28]. DL technology can automatically analyze fetal MRI images to overcome the shortcomings of these traditional methods and improve the early diagnostic rate for FGR.

Consistent with comparisons to manual assessment, the DL system's superiority in FGR diagnosis may originate from its ability to automatically identify features in complex situations, especially through image denoising and edge contrast enhancement [12]. In future clinical applications, DL-assisted fetal MRI assessment can significantly improve the accuracy of early diagnosis. It can display huge potential when it comes to regions with limited resources or environments with low technological levels.

Limitations

Although this study demonstrated the potential of AIR™ Recon DL in placental segmentation and the assessment of FGR and PI, its clinical implementation still faces several challenges. Despite the improvement in image quality, fetal motion artifacts remain a persistent limitation in fetal MRI, especially during active fetal movement. Furthermore, the evaluation of PI relies not only on imaging quality but also on comprehensive integration with other clinical parameters, such as hemodynamic indices and laboratory data. The retrospective, single-center design of this study and the relatively small sample size may also limit the generalizability of the findings. In addition, the results may be influenced by scanner- and vendor-specific characteristics, as all MRI data were acquired on a single 3.0-T GE SIGNA™ Premier system using the AIR™ Recon DL algorithm. Therefore, caution should be exercised when extrapolating the results to other MRI platforms or reconstruction algorithms. Although ultrasound FL measurements followed ISUOG guidelines and were performed by experienced sonographers, operator- and equipment-related variability could not be completely eliminated, potentially affecting the accuracy of EFW. Future studies involving multiple vendors, standardized multicenter ultrasound protocols, and larger patient cohorts are warranted to further validate the robustness and general applicability of our findings.

With ongoing advancements in technology and imaging hardware, DL–based fetal MRI assessment is expected to further reduce manual intervention, improve efficiency, and enhance diagnostic precision. Such AI-assisted systems hold promise as valuable tools for the early detection and individualized management of high-risk pregnancies.

5. Conclusions

In conclusion, our study shows that fetal MRI combined with AIR™ Recon DL has significant clinical value for the assessment of FGR and PI. This technique enhances image quality and reduces artifacts, with high accuracy in fetal weight prediction, placental segmentation, and FGR detection. Despite remaining challenges, this approach offers strong potential for further refinement and wider clinical application and is likely to become an important tool for the management of high-risk pregnancies.

Availability of Data and Materials

The datasets generated and analyzed during the current study are available from the corresponding author upon reasonable request.

Author Contributions

All authors contributed to the study conception and design. YZ and FZ were responsible for material preparation. XL and KL were responsible for data collection. BZ was responsible for data analysis. The first draft of the manuscript was written by YZ, and all authors critically revised the manuscript for important intellectual content. All authors read and approved the final manuscript. All authors have participated sufficiently in the work and agreed to be accountable for all aspects of the work.

Ethics Approval and Consent to Participate

This retrospective study was approved by the Institutional Review Board of the Medical Research Ethics Committee of the Second Hospital of West China, Sichuan University (Approval No. 313, 2024). The requirement for written informed consent was waived due to the retrospective nature of the study. The study was conducted in accordance with the guidelines of the Declaration of Helsinki.

Acknowledgment

The authors would like to thank the radiology and obstetrics teams of the Second Hospital of West China, Sichuan University for their technical assistance and valuable support during data acquisition and analysis.

Funding

This research received no external funding.

Conflict of Interest

The authors declare no conflict of interest.

Declaration of AI and AI-Assisted Technologies in the Writing Process

During the preparation of this work, we used ChatGPT (OpenAI, San Francisco, CA, USA) to assist in checking English grammar and spelling. After using this tool, we carefully reviewed and edited the content to ensure accuracy and appropriateness, and take full responsibility for the content of the publication.

References

[1] Giouleka S, Tsakiridis I, Mamopoulos A, Kalogiannidis I, Athanasiadis A, Dagklis T. Fetal Growth Restriction: A Comprehensive Review of Major Guidelines. Obstetrical & Gynecological Survey. 2023; 78: 690–708. https://doi.org/10.1097/OGX.0000000000001203.

[2] Dall'Asta A, Melito C, Morganelli G, Lees C, Ghi T. Determinants of placental insufficiency in fetal growth restriction. Ultrasound in Obstetrics & Gynecology: the Official Journal of the International Society of Ultrasound in Obstetrics and Gynecology. 2023; 61: 152–157. https://doi.org/10.1002/uog.26111.

[3] Fetal Growth Restriction: ACOG Practice Bulletin, Number 227. Obstetrics and Gynecology. 2021; 137: e16–e28. https://doi.org/10.1097/AOG.0000000000004251.

[4] Wu BA, Chand KK, Bell A, Miller SL, Colditz PB, Malhotra A, *et al*. Effects of fetal growth restriction on the perinatal neurovascular unit and possible treatment targets. Pediatric Research. 2024; 95: 59–69. https://doi.org/10.1038/s41390-023-02805-w.

[5] Melamed N, Baschat A, Yinon Y, Athanasiadis A, Mecacci F, Figueras F, *et al*. FIGO (international Federation of Gynecology and obstetrics) initiative on fetal growth: best practice advice for screening, diagnosis, and management of fetal growth restriction. International Journal of Gynaecology and Obstetrics: the Official Organ of the International Federation of Gynaecology and Obstetrics. 2021; 152 Suppl 1: 3–57. https://doi.org/10.1002/ijgo.13522.

[6] Ohgiya Y, Nobusawa H, Seino N, Miyagami O, Yagi N, Sasamori H, *et al*. MR Imaging of Fetuses to Evaluate Placental Insufficiency. Magnetic Resonance in Medical Sciences. 2016; 15: 212–219. https://doi.org/10.2463/mrms.mp.2015-0051.

[7] Fan H, Li L, Hao C. Clinical significance of three-dimensional power Doppler combined with two-dimensional Doppler ultrasonography for evaluating fetal growth restriction. The Journal of Maternal-fetal & Neonatal Medicine: the Official Journal of the European Association of Perinatal Medicine, the Federation of Asia and Oceania Perinatal Societies, the International Society of Perinatal Obstetricians. 2024; 37: 2322610. https://doi.org/10.1080/14767058.2024.2322610.

[8] Burton CS, Frey K, Fahey F, Kaminski MS, Brown RKJ, Pohlen JM, *et al*. Fetal Dose from PET and CT in Pregnant Patients. Journal of Nuclear Medicine: Official Publication, Society of Nuclear Medicine. 2023; 64: 312–319. https://doi.org/10.2967/jnumed.122.263959.

[9] Malamateniou C, Malik SJ, Counsell SJ, Allsop JM, McGuinness AK, Hayat T, *et al*. Motion-Compensation Techniques in Neonatal and Fetal MR Imaging. AJNR American Journal of Neuroradiology. 2013; 34: 1124–1136. https://doi.org/10.3174/ajnr.A3128.

[10] Salomon LJ, Alfirevic Z, Da Silva Costa F, Deter RL, Figueras F, Ghi T, *et al*. ISUOG Practice Guidelines: ultrasound assessment of fetal biometry and growth. Ultrasound in Obstetrics & Gynecology: the Official Journal of the International Society of Ultrasound in Obstetrics and Gynecology. 2019; 53: 715–723. https://doi.org/10.1002/uog.20272.

[11] Kingdom JC, Audette MC, Hobson SR, Windrim RC, Morgen E. A placenta clinic approach to the diagnosis and management of fetal growth restriction. American Journal of Obstetrics and Gynecology. 2018; 218: S803–S817. https://doi.org/10.1016/j.ajog.2017.11.575.

[12] Ramirez Zegarra R, Ghi T. Use of artificial intelligence and deep learning in fetal ultrasound imaging. Ultrasound in Obstetrics & Gynecology: the Official Journal of the International Society of Ultrasound in Obstetrics and Gynecology. 2023; 62: 185–194. https://doi.org/10.1002/uog.26130.

[13] Scheinost D, Pollatou A, Dufford AJ, Jiang R, Farruggia MC, Rosenblatt M, *et al*. Machine Learning and Prediction in Fetal, Infant, and Toddler Neuroimaging: A Review and Primer. Biological Psychiatry. 2023; 93: 893–904. https://doi.org/10.1016/j.biopsych.2022.10.014.

[14] Specktor-Fadida B, Link-Sourani D, Rabinowich A, Miller E, Levchakov A, Avisdris N, *et al*. Deep learning-based segmentation of whole-body fetal MRI and fetal weight estimation: assessing performance, repeatability, and reproducibility. European Radiology. 2024; 34: 2072–2083. https://doi.org/10.1007/s00330-023-10038-y.

[15] Davidson L, Boland MR. Towards deep phenotyping pregnancy: a systematic review on artificial intelligence and machine learning methods to improve pregnancy outcomes. Briefings in Bioinformatics. 2021; 22: bbaa369. https://doi.org/10.1093/bib/bbaa369.

[16] Heckel R, Jacob M, Chaudhari A, Perlman O, Shimron E. Deep learning for accelerated and robust MRI reconstruction. Magnetic Resonance Materials in Physics, Biology

and Medicine. 2024; 37: 335–368. https://doi.org/10.1007/s10334-024-01173-8.

[17] Zheng W, Jiang Y, Jiang Z, Li J, Bian W, Hou H, *et al*. Association between deep learning radiomics based on placental MRI and preeclampsia with fetal growth restriction: A multicenter study. European Journal of Radiology. 2025; 184: 111985. https://doi.org/10.1016/j.ejrad.2025.111985.

[18] Chlap P, Min H, Vandenberg N, Dowling J, Holloway L, Haworth A. A review of medical image data augmentation techniques for deep learning applications. Journal of Medical Imaging and Radiation Oncology. 2021; 65: 545–563. https://doi.org/10.1111/1754-9485.13261.

[19] Knoll F, Hammernik K, Zhang C, Moeller S, Pock T, Sodickson DK, *et al*. Deep-Learning Methods for Parallel Magnetic Resonance Imaging Reconstruction: A Survey of the Current Approaches, Trends, and Issues. IEEE Signal Processing Magazine. 2020; 37: 128–140. https://doi.org/10.1109/MSP.2019.2950640.

[20] Sobhaninia Z, Rafiei S, Emami A, Karimi N, Najarian K, Samavi S, *et al*. Fetal Ultrasound Image Segmentation for Measuring Biometric Parameters Using Multi-Task Deep Learning. Annual International Conference of the IEEE Engineering in Medicine and Biology Society. IEEE Engineering in Medicine and Biology Society. Annual International Conference. 2019; 2019: 6545–6548. https://doi.org/10.1109/EMBC.2019.8856981.

[21] Cha SH, Han YE, Han NY, Kim MJ, Park BJ, Sim KC, *et al*. Assessing Image Quality in Multiplexed Sensitivity-Encoding Diffusion-Weighted Imaging with Deep Learning-Based Reconstruction in Bladder MRI. Diagnostics (Basel, Switzerland). 2025; 15: 595. https://doi.org/10.3390/diagnostics15050595.

[22] Lee KL, Kessler DA, Dezonie S, Chishaya W, Shepherd C, Carmo B, *et al*. Assessment of deep learning-based reconstruction on T2-weighted and diffusion-weighted prostate MRI image quality. European Journal of Radiology. 2023; 166: 111017. https://doi.org/10.1016/j.ejrad.2023.111017.

[23] Chen Z, Pawar K, Ekanayake M, Pain C, Zhong S, Egan GF. Deep Learning for Image Enhancement and Correction in Magnetic Resonance Imaging—State-of-the-Art and Challenges. Journal of Digital Imaging. 2023; 36: 204–230. https://doi.org/10.1007/s10278-022-00721-9.

[24] Zerunian M, Pucciarelli F, Caruso D, Polici M, Masci B, Guido G, *et al*. Artificial intelligence based image quality enhancement in liver MRI: a quantitative and qualitative evaluation. La Radiologia Medica. 2022; 127: 1098–1105. https://doi.org/10.1007/s11547-022-01539-9.

[25] Kim JH, Yoon JH, Kim SW, Park J, Bae SH, Lee JM. Application of a deep learning algorithm for three-dimensional T1-weighted gradient-echo imaging of gadoxetic acid-enhanced MRI in patients at a high risk of hepatocellular carcinoma. Abdominal Radiology (New York). 2024; 49: 738–747. https://doi.org/10.1007/s00261-023-04124-4.

[26] Peterson HF, Eskild A, Sommerfelt S, Gjesdal K, Borthne AS, Mørkrid L, *et al*. Percentiles of intrauterine placental volume and placental volume relative to fetal volume: A prospective magnetic resonance imaging study. Placenta. 2022; 121: 40–45. https://doi.org/10.1016/j.placenta.2022.02.023.

[27] Konwar R, Basumatary B, Dutta M, Mahanta P. Accuracy of Fetal Weight Estimation by Ultrasonographic Evaluation in a Northeastern Region of India. International Journal of Biomaterials. 2021; 2021: 9090338. https://doi.org/10.1155/2021/9090338.

[28] Tsikouras P, Antsaklis P, Nikolettos K, Kotanidou S, Kritsotaki N, Bothou A, *et al*. Diagnosis, Prevention, and Management of Fetal Growth Restriction (FGR). Journal of Personalized Medicine. 2024; 14: 698. https://doi.org/10.3390/jpm14070698.